Advancing Autreasery and Geophysics

Modulated accretion in the T Tauri star RY Tau – a stable MHD propeller or a planet at 0.2 au?

P. P. Petrov , 1 M. M. Romanova, K. N. Grankin, S. A. Artemenko, E. V. Babina and S. Yu. Gorda

Accepted 2021 March 26. Received 2021 March 24; in original form 2021 January 8

ABSTRACT

Planets are thought to form at the early stage of stellar evolution when mass accretion is still ongoing. RY Tau is a T Tauri type star at the age of a few Myr, with an accretion disc seen at high inclination, so that the line of sight crosses both the wind and accretion gas flows. In a long series of spectroscopic monitoring of the star over the period 2013–2020, we detected variations in H α and Na I D absorptions at radial velocities of infall (accretion) and outflow (wind) with a period of about 22 d. The absorptions in the infalling and outflowing gas streams vary in antiphase: an increase of infall is accompanied by a decrease of outflow, and vice versa. These 'flip-flop' oscillations retain phase over several years of observations. We suggest that this may result from the magnetohydrodynamics processes at the disc–magnetosphere boundary in the propeller mode. Another possibility is that a massive planet is modulating some processes in the disc and is providing the observed effects. The period, if Keplerian, corresponds to a distance of 0.2 au, which is close to the dust sublimation radius in this star. The presence of the putative planet can be confirmed by radial velocity measurements: the expected amplitude is ≥ 90 m s⁻¹ if the planet mass is ≥ 2 M_J.

Key words: line: profiles – stars: individual: RY Tau – stars: variables: T Tauri, Herbig Ae/Be – stars: winds, outflows.

1 INTRODUCTION

Accretion plays a major role in the observed properties of classical T Tauri stars (CTTS), which are low-mass (<2–3 M_{\odot}) stars at the early stage of their evolution; see reviews by Bouvier et al. (2007) and Hartmann, Herczeg & Calvet (2016). CTTS host accretion discs, where planetary system formation is going on. In recent years, the ALMA interferometer has provided new evidence of the planetary formation processes around CTTS (e.g. Dong, Najita & Brittain 2018).

The observed activity of CTTS, including their rich emission-line spectrum and irregular light variability, is a result of magnetospheric accretion, wind outflow and the dusty circumstellar environment. Accretion is a driving force of most of these processes. Both accretion and wind flows are non-stationary, which makes the investigation challenging. Magnetospheric accretion works in different astrophysical objects: neutron stars, white dwarfs in cataclysmic variables, and young stars. Accretion in young stars is relatively slow, compared with that in compact objects. Therefore, a classical T Tauri star is a convenient laboratory to study accretion in detail. In parallel to observations, numerical simulations of the accretion and winds in a variety of astrophysical objects have helped us make significant progress (see a review by Romanova & Owocki 2015).

From spectroscopic observations, the direction and velocity of the gas flows around CTTS can be traced from emission and absorption line profiles broadened by the Doppler effect. In the visual spectrum,

the H α line profile is the main indicator of wind, while the redshifted absorptions formed in the accretion funnels are most visible in Na I D and the O I 7773 triplet lines. A reach sample of the inversed P Cyg profiles of metal lines was observed in the classical T Tauri star, S CrA SE (Petrov et al. 2014). A combination of spectroscopy and photometry provides information about the flux variability in emission lines.

At the Crimean Astrophysical Observatory (CrAO), we have carried out a long monitoring programme of two CTTS: RY Tau and SU Aur. The aim is to follow the dynamics of accretion and wind flows on time-scales from days to years. A major part of the programme has been published in Petrov et al. (2019), hereafter referred to as Paper I. Now we present new results, including the seasons of 2018–2019 and 2019–2020, with emphasis on the discovery of modulated accretion and wind flows around RY Tau.

RY Tau is one of the brightest and most studied CTTS. With stellar mass $M=2.08\,\mathrm{M}_\odot$, luminosity $L=13.5\,\mathrm{L}_\odot$ and $T_\mathrm{eff}=5945\,\mathrm{K}$ (Paper I), the star is between CTTS and the more massive Herbig Ae/Be stars The mass accretion rate, estimated from ultraviolet (UV) luminosity, is 6.4-9.1 in units of $10^{-8}\,\mathrm{M}_\odot$ yr⁻¹ (Calvet et al. 2004). From the ALMA survey of protoplanetary discs around young stars (Long et al. 2019), the accretion disc of RY Tau is seen at high inclination, $i=65^\circ\pm0^\circ.1$, so that the line of sight to the star intersects the wind flows, the dusty atmosphere of the inner disc, and the accretion funnels within the magnetosphere. The irregular variability of the brightness is mostly a result of circumstellar extinction (Babina, Artemenko & Petrov 2016). Evidence of stellar occultation by the disc atmosphere close to the sublimation rim at 0.2 au from the star was received from K-band interferometry (Davies et al. 2020).

¹Crimean Astrophysical Observatory, p/o Nauchny, 298409, Republic of Crimea

²Cornell University, Ithaca, NY 14853, USA

³Ural Federal University, 51 Lenin av., Ekaterinburg, 620000, Russia

^{*} E-mail: petrov@craocrimea.ru

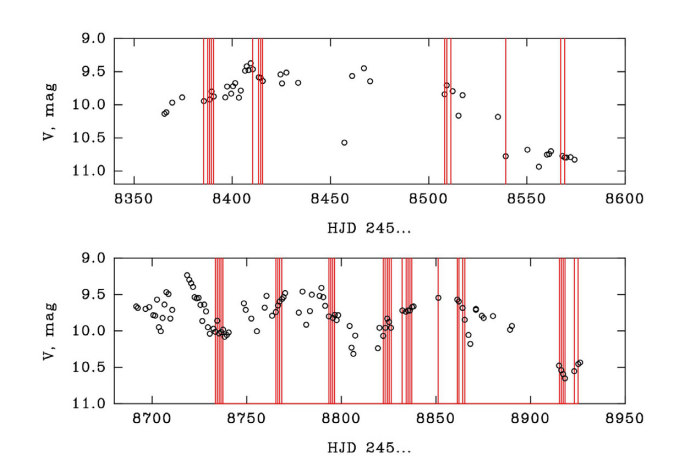


Figure 1. Light curve of RY Tau in two seasons, 2018–2019 (upper panel) and 2019–2020 (lower panel). Vertical lines mark the moments of spectral observations.

No rotational modulation of brightness was detected, with a certain confidence, in the extended photometric series of RY Tau, although some quasi-periods were reported (e.g. Herbst et al. 1987; Zajtseva 2010). From the stellar parameters and the observed $v \sin i = 52 \pm 2 \,\mathrm{km \, s^{-1}}$ (Bouvier 1990; Petrov et al. 1999), and assuming the inclination $i = 65^\circ$ (the same as in the accretion disc), the period of the axial rotation should be about 3 d (i.e. RY Tau is a fast rotator). RY Tau has an extended jet with a few knots of young dynamical ages (St-Onge & Bastien 2008). The jet is wiggled, which was interpreted as resulting from the presence of an unseen planetary or substellar companion to the star (Garufi et al. 2019).

The interferometric image of the protoplanetary disc around RY Tau at millimetre wavelengths did not reveal planets more massive than 5 M_J at distances between 10 and 60 au (Isella, Carpenter & Sargent 2010).

This paper is organized as follows. First, we describe briefly the instruments and observation sites and outline the amount of data collected. Then we analyse the variability of H α and Na I D lines in terms of accretion and wind flows, with emphasis on the 'flip-flop' effect. Finally, we discuss the results in terms of the propeller regime with the possible presence of a planet.

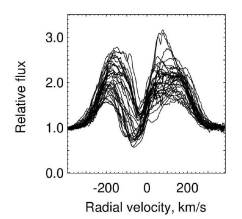
2 OBSERVATIONS

Our programme of spectral and photometric monitoring of RY Tau has been underway since 2013. A description of the telescopes and instruments at different observatories, used in this monitoring, is given in Paper I. The major part of the spectroscopic data was obtained at the CrAO with an echelle spectrograph at the 2.6-m Shajn reflector. The registered spectral regions included H α and Na I D lines, with resolution $\lambda/\Delta\lambda=27\,000$.

So far, we have collected over 160 nights of spectral observations of RY Tau during seven seasons, from 2013 to 2019. The light curves for the latest two seasons are presented in Fig. 1, where the moments of spectral observations are marked with vertical bars. The light curves and moments of spectral observations in the previous five seasons from 2013 to 2018 are given in Paper I.

3 RESULTS

In the following, we analyse the variability of the $H\alpha$ and NaI D lines and we interpret the results in terms of the accretion and



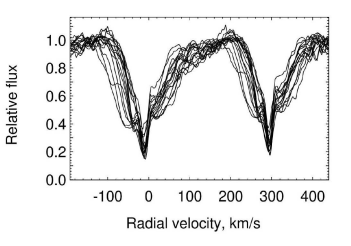


Figure 2. The variability ranges of H α emission (left) and Na I D absorption (right) profiles in 2019–2020. In the region of Na I D lines, the radial velocity scale is given for the D2 line.

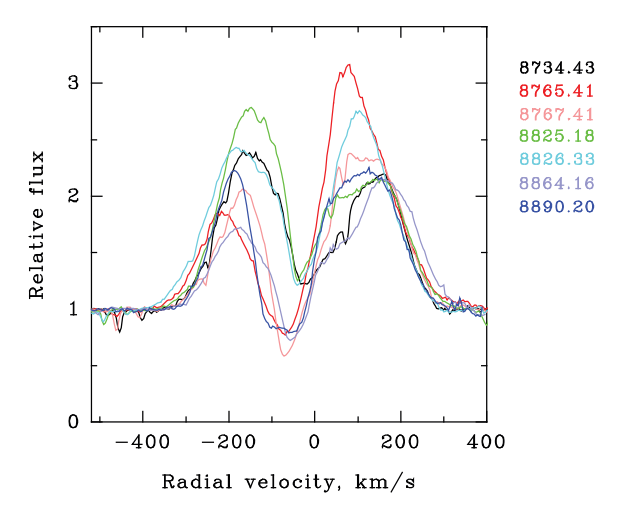


Figure 3. Sample of $H\alpha$ line profiles. Observation dates are displayed in the same colour as the corresponding profiles.

wind gas flows. The H α emission line has a broad profile with variable depression in the blue wing, sometimes below continuum, indicating absorption in the outflowing gas. The red wing is also variable in the intensity of emission. The Na I D lines show a profile composed of several components: photospheric absorption of a G2 type star, broadened by axial rotation to $v \sin i = 52 \pm 2 \text{ km s}^{-1}$: a narrow absorption dip of interstellar origin; and broad variable absorptions in the blue and red wings. As an example, Fig. 2 shows the variability ranges of the Hα and Na I D line profiles, observed in one season of 2019-2020. In this and the following diagrams, the radial velocity is astrocentric, assuming the heliocentric radial velocity of RY Tau is $+18.0 \text{ km s}^{-1}$ (Petrov et al. 1999). The terms 'blue' and 'red' wings of a line correspond to negative and positive radial velocities, respectively. Another example is shown in Figs 3 and 4, where the observation dates are colour coded so the line changes over time can be traced.

Besides the intrinsic variability of the H α flux, the observed intensity of H α emission depends on the circumstellar extinction: when the brightness of RY Tau drops, the equivalent width (EW) of H α emission becomes higher (Paper I). This may be because circumstellar dust obscures the star, but not the whole area of H α emission. In this case, the total flux radiated in H α can be calculated as $F = \text{EW} \times 10^{-0.4(V-10)}$, where the flux is expressed in units of the continuum flux density of a star with V = 10 mag, which is 3.67×10^{-13} erg cm⁻² s⁻¹ Å⁻¹. The photometric R band would be more appropriate for H α flux calibration, but for some moments of spectral observations only V magnitudes are available. In RY Tau, the colour (V - R) does not change considerably with brightness: on

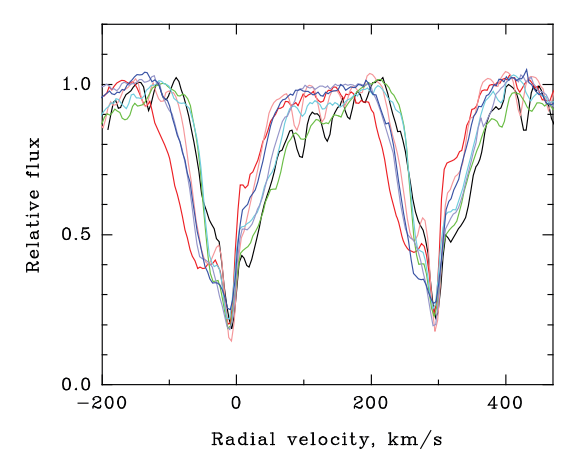


Figure 4. Sample of Na I D line profiles. Observation dates and colours are the same as in Fig. 3.

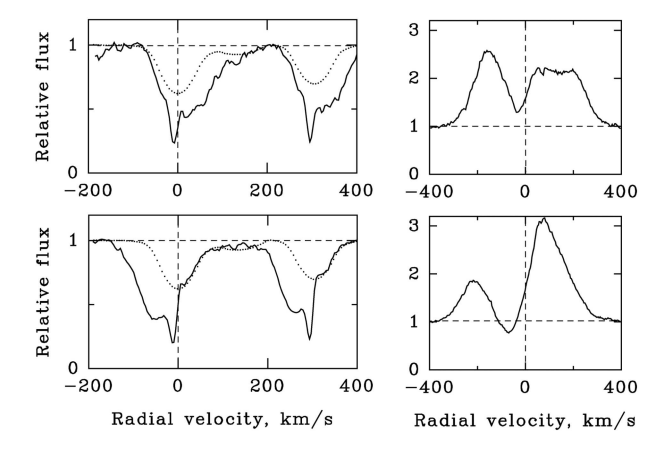


Figure 5. Na I D and H α line profiles on different dates, HJD = 245 8737.41 (upper) and 245 8765.42 (lower). The photospheric components of the Na I D absorptions, broadened by stellar rotation to $v \sin i = 52 \,\mathrm{km \, s^{-1}}$, are shown as dotted profiles. The absorption dip at about zero velocity in the Na I D profile belongs to interstellar absorption.

average, $(V - R) = 1.1 \pm 0.1$ mag. Therefore, the use of V magnitude introduces a constant factor to the derived flux.

The accretion and wind gas flows affect the red and blue wings of spectral lines, broadened by the Doppler effect. For H α , the major changes are in the depth of blueshifted absorption, while in the Na_I D lines varying absorptions appear on the blue or red sides of the photospheric component. The most clear example of such a variability in H α and Na_I D lines is shown in Fig. 5.

In the Na1D2 line, we measure the equivalent widths of the blue and red wings, D2b and D2r, in radial velocity ranges [-160, -10] and [+10, +160] km s $^{-1}$, respectively (i.e. avoiding the central absorption dip of circumstellar origin). The photospheric component of D2 contributes constant additions to the variable D2b and D2r quantities.

It was found that D2b and D2r vary in antiphase: an increase in the blueshifted absorption is followed by a decrease of the redshifted absorption, and vice versa. The inverse correlation between the two components is shown in Fig. 6. An example of time variability of D2b and D2r during one season of observations of 2019–2020 is shown in Fig. 7.

In terms of gas flows, these results mean that either inflow or outflow prevails on the line of sight at any moment of observation. An

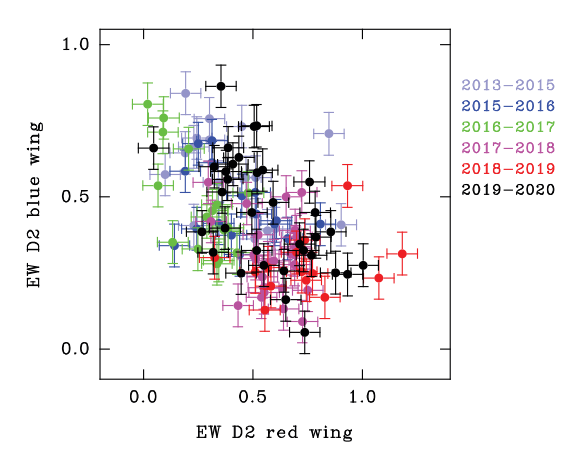


Figure 6. Inverse correlation between equivalent widths (EW, Å) of the blue and red wings of D2 absorption. The different seasons of observations are colour coded.

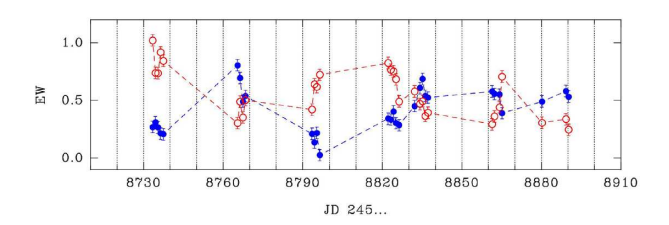


Figure 7. Antiphase variations of equivalent widths (EW, Å) of the blue (filled circles) and red (open circles) wings of the D2 absorption during the season of 2019–2020.

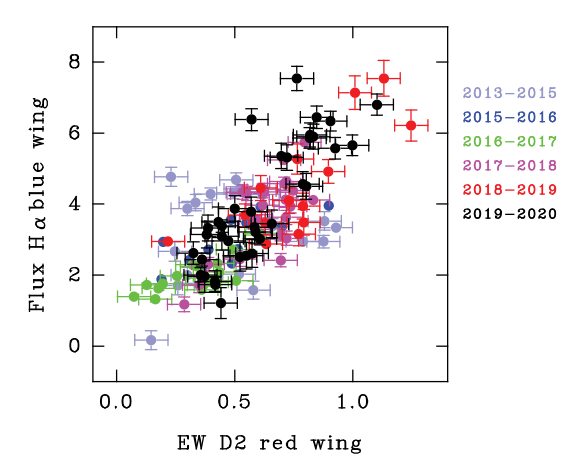


Figure 8. Correlation in the variability of equivalent width (EW, Å) of the red wing of Na₁D2 absorption and the flux in the blue wing of H α emission. The flux units are 3.67 \times 10⁻¹³ erg cm⁻² s⁻¹. The different seasons of observations are colour coded.

even more tight correlation appears in the variability of the red wing of Na I D2 absorption and the flux in the blue wing of H α emission (Fig. 8). An increase of absorption in the red wing of Na I D2 is accompanied by an increase of emission in the blue wing of H α . The blue wing of H α is the best indicator of outflow: the increase of emission flux in the H α blue wing means fading of the wind. However, the increase of absorption in the red wing of the D2 line signals the appearance of infalling gas on the line of sight. Therefore, the correlation in Fig. 8 also indicates the inverse correlation between inflow and outflow on the line of sight.

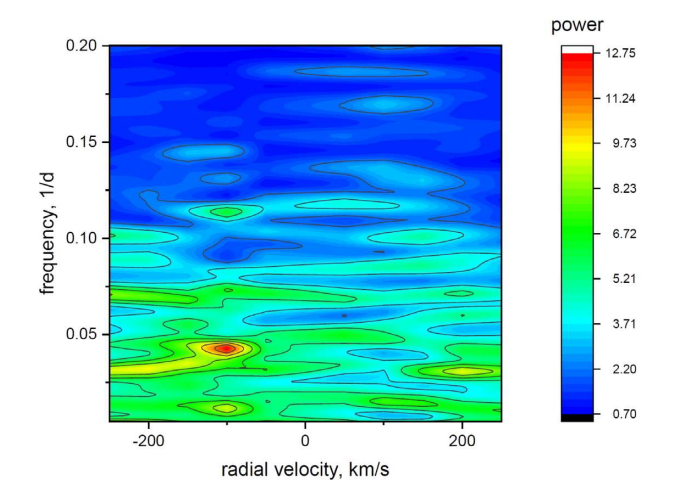


Figure 9. A 2D periodogram of the H α flux. The maximum power is concentrated at radial velocity $-100~\rm km\,s^{-1}$, at a frequency of about 0.04, corresponding to a period within 22–24 d.

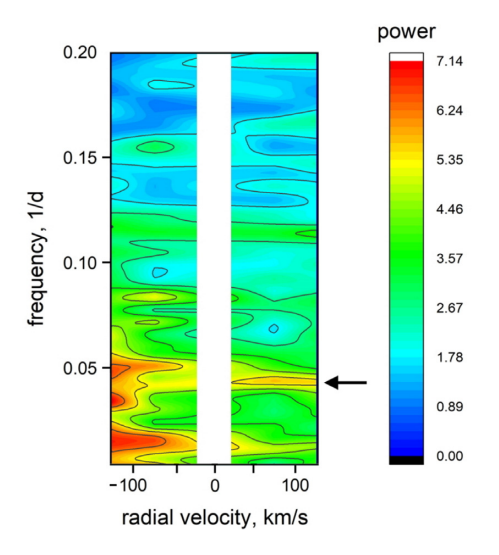


Figure 10. A 2D periodogram of the Na I D2 intensity. The central blank strip is the excluded region of interstellar absorption. Note the enhanced power in the red wing of the line at the frequency of 0.044 (marked with an arrow), corresponding to a period of 22.7 d.

The red wing of H α emission does not correlate with any part of the Na I D2 absorption.

In the following, we analyse time variability in the H α and D2 line profiles. The time series of H α profiles includes 162 nights of observations in 2013–2010. The H α emission is strong and easy to measure in each spectrum, while the D2 absorption profile in some spectra appears noisy, or contaminated by water lines; therefore, there are fewer Na I D spectra used in the analysis, about 120. The variables are fluxes in the H α emission line profile and intensities in the Na I D2 line profile. The Lomb–Scargle algorithm modified by Horne & Baliunas (1986) was applied.

Figs 9 and 10 show a two-dimensional (2D) periodogram in the ranges of periods longer than 5 d and the ranges of radial velocities from -250 to +250 km s⁻¹ in H α and from -125 to +125 km s⁻¹ in the Na₁D2 line. In the H α emission periodogram, there is a clear spot of high power at the radial velocity of -100 km s⁻¹, at the frequency of about 0.04 d⁻¹, corresponding to a period within

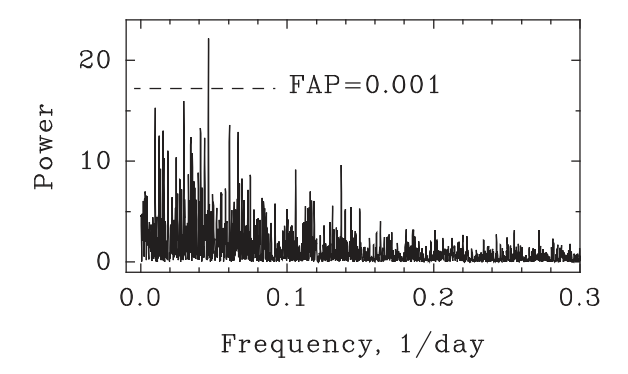


Figure 11. Power spectrum of $H\alpha$ line asymmetry. The highest peak corresponds to the period of 21.6 d.

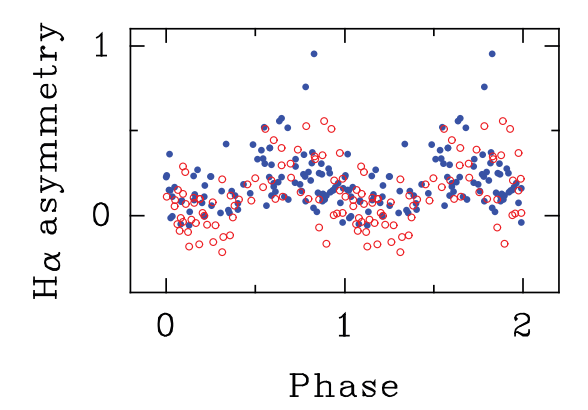


Figure 12. H α line asymmetry convolved with a period of 21.6 d. Asymmetry = 1 corresponds to the P Cyg type profile. Filled and open circles denote data from 2013–2017 and 2017–2020, respectively. The origin of time is the same in both samples: HJD = 245 6592.444.

22-24 d. At the same frequency, the highest power is observed in the red wing of the Na_ID2 line. Unlike H α , the periodic modulation of the Na_ID2 line is not confined to a narrow radial velocity range, but is observed across the red wing of the line, from +50 to +150 km s $^{-1}$, at the frequency of 0.044 \pm 0.002 d $^{-1}$, which corresponds to a period of 22.7 \pm 1.0 d. In the blue wing of the Na_ID2 line, this period is blended with others in the range of 20–30 d. Note that the absorption features measured in Na_ID are relatively small and prone to errors, because of the presence of telluric water lines.

The periodic variations in H α can be revealed also in an analysis of the line profile asymmetry. As a line asymmetry, we use the difference-to-sum ratio (b-r)/(b+r), where b and r are the equivalent widths of the blue and red halves of the line profile relative to zero radial velocity. Asymmetry = 1 corresponds to the P Cyg profile, and asymmetry = 0 corresponds to symmetric blue and red wings. The power spectrum of the H α line asymmety in the full set of our observations of RY Tau (seven seasons) reveals oscillations with the most probable period of 21.6 d, with false alarm probability FAP < 0.001 (see Fig. 11). Fig. 12 shows the phase diagram of H α asymmetry. The data are split into two parts: 2013–2017 (93 dates of observations) and 2017–2020 (69 dates) to show that oscillations were present in both parts.

The periodic variation in the blue wing of H α occurs at a radial velocity of about $-100~\rm km~s^{-1}$, which is within the wide blueshifted dip associated with the wind. Fig. 3 shows that the radial velocity of $-100~\rm km~s^{-1}$ falls within the steep slope of the dip, so the observed

variations of line intensity at this part of the profile may be caused by changes in the outflow velocity.

In the Na_I D lines, the variable absorption in the red wing is formed in the infalling gas. The infall velocity range from +50 to +150 km s⁻¹ covers almost the whole accretion channel within the magnetosphere. The oscillations in the red wing of Na_I D mean that we observe modulated accretion.

4 DISCUSSION

The emission line profiles broadened by the Doppler effect provide information about the main directions of gas flows – accretion and wind (Hartmann 1998; Alencar & Basri 2000). The models of magnetospheric accretion and the disc wind were used to interpret the observed profiles of H I and He I (Kurosawa, Harries & Symington 2006; Kurosawa, Romanova & Harries 2011; Kwan & Fischer 2011; Gahm et al. 2018). The dynamics of wind in CTTS was studied in a number of spectral time series (e.g. Giampapa et al. 1993; Johns & Basri 1995; Alencar, Johns-Krull & Basri 2001; Alencar et al. 2005; Takami et al. 2016; Paper I).

Periodic variations in the accretion and wind features were first detected in the spectrum of SU Aur (Giampapa et al. 1993; Johns & Basri 1995), which is a fast rotating TTS with stellar parameters resembling those of RY Tau. Johns & Basri (1995) suggested a model of an oblique rotator (the 'eggbeater' model) to explain how the wind and accretion flows replace each other on the line of sight as the star rotates. More advanced models were elaborated later to explain the observed periodic modulations in the photometric and spectroscopic features in CTTS. If the large-scale stellar magnetosphere is inclined on to the stellar rotational axis, the interaction of the magnetic field with the inner disc results in the formation of a strong bending wave (a warp). The warp is close to the radius of corotation and rotates with the angular velocity of the star, like the warp observed in AA Tau (Bouvier et al. 1999, 2013), and the warps observed in the global three-dimensional simulations (Romanova et al. 2013).

In the case of RY Tau, the observed 22-d period is much longer than the 3-d period of stellar rotation, so the model of the inclined magnetosphere cannot be applied. For the first time, the periodic switches of the accretion and wind flows, not related to stellar rotation, have been observed in a classical T Tauri star. An interpretation of this phenomenon should answer the following question. Is this an intrinsic property of the magnetospheric accretion process, or is it induced by an external force, such as the orbital motion of a planet or a substellar companion?

A powerful instrument for the analysis of the gas flows around a young star is the numerical simulation of the accretion and winds (see a review by Romanova & Owocki 2015). Formulation of the basic concepts can be found in Camenzind (1990), Shu et al. (1994) and Lovelace, Romanova & Bisnovatyi-Kogan (1995).

In CTTS, the accretion and winds are physically related processes, where the winds are consequences of accretion – either magnetospheric accretion or disc accretion. Although the magnetic fields of CTTS are multipolar, it is the dipole mode that truncates the accretion disc and controls the magnetospheric accretion (Johnstone et al. 2014).

The main parameters that determine the modes of accretion and wind are stellar mass M, the angular velocity of rotation of the star Ω , the magnetic field of the star (the magnetic moment of the dipole μ) and the mass accretion rate \dot{M} . With these parameters, the corotation radius $R_{\rm co}$ and the radius of stellar magnetosphere $R_{\rm m}$ are expressed as $R_{\rm co}^3 = G M/\Omega^2$ and $R_{\rm m} \approx \mu^{4/7}/(\dot{M}^2 G M)^{1/7}$ (Koenigl 1991). The

condition $R_{co} = R_{m}$ defines the boundary between the accretion regime and the propeller regime (Romanova & Owocki 2015).

In the case of the fast rotating RY Tau, $R_{\rm co} \approx 3~R_{\rm star}$. The magnetospheric radius of a classical T Tauri star is typically about 7 stellar radii (Bouvier et al. 2007), although it can be within 3–10 in individual stars (Johnstone et al. 2014). RY Tau is most probably in the propeller regime. The presence of the extended jet in RY Tau is evidence in favour of a strong propeller.

In the propeller regime, the condition $R_{\rm m} > R_{\rm co}$ does not prevent the accretion completely, but makes it non-permanent. The centrifugal barrier prevents the accretion of matter in the equatorial plane. However, the matter may flow above or below the closed parts of the magnetosphere and accrete on to a star from poles.

Axisymmetric simulations show the presence of both accretion and outflows during the propeller regime (e.g. Romanova et al. 2005, 2009; Ustyugova et al. 2006). Matter accretes inward, accumulates in the inner disc and diffusively penetrates through the external layers of the closed magnetosphere. When some critical amount of matter accumulates inside the magnetosphere and the centrifugal force becomes larger than the magnetic tension force, the closed field lines inflate, and the accumulated matter expels in the wind. At the same time, matter accretes on to a star from the opposite side of the disc, where the magnetosphere is closed (Lii et al. 2014; Romanova et al. 2018). The process is cyclic. After unloading matter, the inner disc becomes 'lighter', and the magnetosphere expands and pushes the inner disc outward. After this, the process of accumulation/diffusion repeats.¹

The time-scale and the level of periodicity between the accretion/ejection events depend on several factors, including the viscosity (accretion rate) in the disc and diffusivity at the disc-magnetosphere boundary. For example, at small values of diffusivity, $\alpha = 0.02$ (used in Romanova et al. 2018), events of accretion/ejection are episodic, and only occasionally quasi-periodic. However, in experimental simulations of accretion at higher values of diffusivity, $\alpha_d = 0.2$ and viscosity $\alpha_v = 0.6$ in the disc, these events become almost periodic (see fig. 3 of Romanova et al. 2005). Goodson, Winglee & Bohm (1997) and Zanni & Ferreira (2009) also used relatively high viscosity and diffusivity ($\alpha_d = 0.2$ and 1.0, respectively), and observed almost periodic events of inflation of the magnetic field lines and ejections to the wind in non-propelling stars. All the above simulations are axisymmetric, and exclude important instabilities at the disc-magnetosphere boundary, such as Rayleigh-Taylor instability. Three-dimensional simulations of accretion in the nonpropeller regime show that this instability provides highly efficient diffusivity at the disc-magnetosphere boundary (e.g. Romanova & Owocki 2015). We suggest that accretion/ejection events could be more periodic in the more realistic case of higher diffusivity.

With application to RY Tau, the axisymmetric simulations show episodic or quasi-periodic ejections with time-scales of 10–100 d, depending on the parameters of the model. Global three-dimensional MHD simulations of the propeller regime are required to understand whether these ejections can be periodic. Magnetic fields of some TTS are known to change on a time-scale of years (e.g. Donati et al. 2011; Yu et al. 2019), so the characteristic time of the quasi-periodic ejections may be slowly variable.

Another characteristic of the propeller is that the direction of the accretion funnel (and outflows) switches between upward and

¹Cyclic accretion and ejection were observed by Goodson et al. (1997) and Zanni et al. (2007) in a non-propeller regime, where the cycle is connected with periodic inflation of the field lines (see also Lovelace et al. 2010).

downward relative to the disc plane (Lovelace et al. 2010). In this case, on the line of sight to the star, one should observe alternation of the wind and accretion features. This seems to be a reasonable explanation of the observed 'flip-flops' of accretion and wind flows in RY Tau, but this scenario is not perfect either. Because of the inherent turbulence of the gas flows, the actual direction of the accretion funnel (above or below the disc plane) in each cycle cannot be predicted. The numerical simulations show that the path of the accretion is not necessarily changed in each cycle: a new cycle can start with the same direction, and the oscillation phase is not preserved. In this case, one cannot expect the phase diagram to be like that in Fig. 12.

Alternatively, the stable cycling of the accretion/ejection events may be induced by a planet orbiting near the inner edge of the accretion disc. This scenario has not been studied in detail by numerical simulations, except for the research by Teyssandier & Lai (2020), where it was first shown how the accretion rate at the inner disc edge is regulated by a massive planet at excentric orbit.

A period of about 23 d in variations of emission-line intensities in the UV and optical spectra of RY Tau was reported earlier by Ismailov et al. (2011) and interpreted as a consequence of a protoplanet orbiting in the inner accretion disc. The presence of a planet or a substellar companion to RY Tau has also been suggested from the fact that jet of the star is wiggled. Garufi et al. (2019) estimated that the observed amount of the jet wiggle is consistent with the presence of a precessing disc warp or misaligned inner disc that would be induced by a gravitating object – a giant planet or a substellar companion. The relation between the mass and orbital distance of a putative planet responsible for the jet wiggle in RY Tau (see fig. 6 in Garufi et al. 2019) indicates that it may be a planet with mass 3–4 M_J at a distance of about 0.2 au.

One may expect that the disc warp or inclined inner disc could be noticed from the photometric series of the star. The near-infrared interferometry of RY Tau has shown that the star is occulted by the disc surface layers close to the sublimation rim (Davies et al. 2020). A similar conclusion was made from the photometric data: the star is permanently obscured by the dusty disc wind, with minimal circumstellar extinction Av = 1.6 mag (Paper I). Analysis of a long photometric series of RY Tau (Artemenko, Grankin & Petrov 2010) did not reveal any stable period around 22 d, although the 20-d period was noticed earlier in the photometric observation of 1993 (Zajtseva 2010). Probably, the distortions of the inner disc, associated with the putative planet, are mostly within the sublimation radius, in a dust-free zone.

With the mass of RY Tau (i.e. $2.08~{\rm M}_{\odot}$), the period of 22 d corresponds to a Keplerian orbit at 0.2 au. The inclination angle of RY Tau ($i=65^{\circ}$) enables us to confirm the planet with the radial velocity technique; the expected amplitude is $\geq 90~{\rm m~s}^{-1}$ if the planet mass is $\geq 2~{\rm M}_{\rm J}$.

5 CONCLUSIONS

The monitoring of RY Tau over 7 yr has revealed a highly probable period of $\sim\!22\,d$ in variations of spectroscopic signatures of accretion and wind in H α and Na I D line profiles. The absorptions in the infalling and outflowing gas streams vary in antiphase: an increase of infall is accompanied by a decrease of outflow, and vice versa. The period that is found is much longer than that of the axial rotation of the star. If Keplerian, the period corresponds to a distance of 0.2 au, which is close to the dust sublimation radius in this star. Although the oscillations of the accretion and wind flows may be explained by the MHD processes at the disc–magnetosphere boundary in the propeller regime, the phase stability of the observed modulations suggests the

effect of an external force. As a tentative interpretation, we suggest a gravitational effect of a planet orbiting at 0.2 au.

The presence of the putative planet may be confirmed by radial velocity measurements: the expected amplitude is $\geq 90~\text{m s}^{-1}$ if the planet mass is $\geq 2~M_J$. Alternatively, if a more extended series of observations reveals a change in the modulation period, the planet hypothesis will be ruled out.

ACKNOWLEDGEMENTS

The Crimean observations in 2019–2020, including data processing and data analysis by SAA, EVB and PPP, were supported by a grant from the Russian Science Foundation 19-72-10063. MMR acknowledges the National Science Foundation grant AST-2009820. KNG acknowledges partial support from the Ministry of Science and Higher Education of the Russian Federation (grant 075-15-2020-780). SYuG was supported in part by the Ministry of Science and Higher Education of the Russian Federation within the framework of the research activities (project no. FEUZ-2020-0030).

DATA AVAILABILITY STATEMENT

The data underlying this article will be shared on reasonable request to the corresponding author [PP].

REFERENCES

Alencar S., Basri G., 2000, AJ, 119, 1881

Alencar S., Johns-Krull C. M., Basri G., 2001, AJ, 122, 3335

Alencar S., Basri G., Hartmann L., Calvet N., 2005, A&A, 440, 595

Artemenko S. A., Grankin K. N., Petrov P. P., 2010, Astron. Rep., 54, 163

Babina E., Artemenko S., Petrov P., 2016, Astron. Lett., 42, 193

Bouvier J., 1990, AJ, 99, 946

Bouvier J. et al., 1999, A&A, 349, 619

Bouvier J., Alencar S., Harries T., Johns-Krull C. M., Romanova M. M., 2007, in Reipurth B., Jewitt D., Keil K., eds, Protostars and Planets V. University of Arizona Press, Tuscon, AZ, p. 479

Bouvier J., Grankin K., Ellerbroek L. E., Bouy H., Barrado D., 2013, A&A, 557, 77

Calvet N., Muzerolle J., Briceno C., Hernandez J., Hartmann L., Saucedo J. L., Gordon K. D., 2004, AJ, 128, 1294

Camenzind M., 1990, Rev. Mod. Astron., 3, 234

Davies C. L. et al., 2020, ApJ, 897, 31

Donati J. F. et al., 2011, MNRAS, 412, 2454

Dong R., Najita J. R., Brittain S., 2018, ApJ, 862, 103

Gahm G. F., Petrov P. P., Tambovsteva L. V., Grinin V. P., Stempels H. C., Walter F. M., 2018, A&A, 614, 117

Garufi A. et al., 2019, A&A, 628, 68

Giampapa M., Basri G., Johns C. M., Imhoff C., 1993, ApJS, 89, 321

Goodson A. P., Winglee R. M., Bohm K.-H., 1997, ApJ, 489, 199

Hartmann L., 1998, Accretion Processes in Star Formation. Cambridge University Press, Cambridge

Hartmann L., Herczeg G., Calvet N., 2016, ARA&A, 54, 135

Herbst W. et al., 1987, AJ, 94, 137

Horne J. H., Baliunas S. L., 1986, ApJ, 302, 757

Isella A., Carpenter J. M., Sargent A. I., 2010, ApJ, 714, 1746

Ismailov N. Z., Shustarev P. N., Adigezalzade A. N., Bahaddinova G. R., 2011, Astron. Lett., 37, 783

Johns C., Basri G., 1995, AJ, 109, 2800

Johnstone C. P., Jardine M., Gregory S. G., Donati J. F., Hussain G., 2014, MNRAS, 437, 3202

Koenigl A., 1991, ApJ, 370, L39

Kurosawa R., Harries T. J., Symington N. H., 2006, MNRAS, 370, 580

Kurosawa R., Romanova M. M., Harries T. J., 2011, MNRAS, 416, 2623

Kwan J., Fischer W., 2011, MNRAS, 411, 2383

Lii P. S., Romanova M. M., Ustyugova G. V., Koldoba A. V., Lovelace R. V. E., 2014, MNRAS, 441, 86

Long F. et al., 2019, ApJ, 882, 49

Lovelace R. V. E., Romanova M. M., Bisnovatyi-Kogan G. S., 1995, MNRAS, 275, 244

Lovelace R. V. E., Romanova M. M., Ustyugova G. V., Koldoba A. V., 2010, MNRAS, 408, 2083

Petrov P., Zajtseva G., Efimov Y., Duemmler R., Ilyin I. V., Tuominen I., Shcherbakov V. A., 1999, A&A, 341, 553

Petrov P. P., Gahm G. F., Herczeg G. J., Stempels H. C., Walter F. M., 2014, A&A, 568, L10

Petrov P. P. et al., 2019, MNRAS, 483, 132 (Paper I)

Romanova M. M., Owocki S. P., 2015, SSRv, 191, 339

Romanova M. M., Ustyugova G. V., Koldoba A. V., Lovelace R. V. E., 2005, ApJ, 635, 165

Romanova M. M., Ustyugova G. V., Koldoba A. V., Lovelace R. V. E., 2009, MNRAS, 399, 1802

Romanova M. M., Ustyugova G. V., Koldoba A. V., Lovelace R. V. E., 2013, MNRAS, 430, 699

Romanova M. M., Blinova A. A., Ustyugova G. V., Koldoba A. V., Lovelace R. V. E., 2018, New Astron., 62, 94

Shu F., Najita J., Ostriker E., Wilkin F., Ruden S., Lizano S., 1994, ApJ, 429, 781

St-Onge G., Bastien P., 2008, ApJ, 674, 1032

Takami M. et al., 2016, ApJ, 820, 139

Teyssandier J., Lai D., 2020, MNRAS, 495, 3920

Ustyugova G. V., Romanova M. M., Koldoba A. V., Lovelace R. V. E., 2006, ApJ, 646, 304

Yu L. et al., 2019, MNRAS, 489, 5556

Zajtseva G., 2010, Ap, 53, 212

Zanni C., Ferreira J., 2009, AA, 508, 1117

Zanni C., Ferreira J., Rosner R., Bodo G., Massaglia S., 2007, A&A, 469, 811

This paper has been typeset from a T_EX/I_TEX file prepared by the author.